THE ASTRONOMICAL JOURNAL, 116:146–162, 1998 July

STAR FORMATION IN AND EVOLUTION OF THE BLUE COMPACT DWARF GALAXY UGC 6456 DETERMINED FROM *HUBBLE SPACE TELESCOPE* IMAGES[1]

ROGER LYNDS
Kitt Peak National Observatory, National Optical Astronomy Observatories,[2] Box 26732, Tucson, AZ 85726; rlynds@noao.edu
ELINE TOLSTOY
Space Telescope European Coordinating Facility, Karl-Schwarzschild-Strasse 2, D-85748 Garching bei München, Germany; etolstoy@eso.org
EARL J. O'NEIL, JR.
Kitt Peak National Observatory, National Optical Astronomy Observatories,[2] Box 26732, Tucson, AZ 85726; oneil@noao.edu
AND
DEIDRE A. HUNTER
Lowell Observatory, 1400 West Mars Hill Road, Flagstaff, AZ 86001; dah@lowell.edu
Received 1997 December 8; revised 1998 April 7

ABSTRACT

Photometry on the *UVI* system has been performed on the resolved stellar content of the blue compact dwarf galaxy UGC 6456 using Wide Field Planetary Camera 2 (WFPC2) images obtained with the *Hubble Space Telescope*. The resulting color-magnitude diagram (CMD) goes to about $V = 27.5$ and reveals not only a young population of blue main-sequence stars and blue and red supergiants, but also an older evolved population of red giants and a fairly well represented asymptotic giant branch. The distance to the galaxy is estimated from the tip of the red giant branch to be 4.5 Mpc, placing it about 1.5 Mpc farther away than the major members of the M81 Group, with which it is usually associated. The youngest stars are generally associated with H II regions shown on our Hα image and are largely confined to the 745 pc field of our PC images. A comparison of their distribution in the CMD with theoretical isochrones suggests ages from 4 to 10 Myr. The population of older stars is found throughout all WFPC2 camera fields and seems to show an elliptical distribution with an aspect ratio of about 2.4 and an exponential falloff in surface density with distance from a center of symmetry that is not far from the centroid of the youngest stars. Theoretical modeling of the CMD at a metallicity of $Z = 0.001$ suggests star formation in the age interval 1–2 Gyr, a strong burst in the interval 600–800 Myr, and a lower rate of star formation up to the present. The evidence is compatible with a scenario beginning with the formation of a population of low-metallicity stars, enriching a major residual of prestellar material that subsequently fueled an active episode of star formation. That burst of star formation must have been particularly spectacular and may be related to the activity we now see in the distant blue dwarf galaxies revealed in deep imaging.

Key words: color-magnitude diagrams — galaxies: dwarf — galaxies: individual (UGC 6456) — galaxies: irregular — stars: AGB and post-AGB

1. INTRODUCTION

UGC 6456 (VII Zw 403) is generally classified as a blue compact dwarf galaxy (BCD). Such galaxies are small, high surface brightness systems characterized by low luminosity ($-13 > M_B > -17$), low metallicity (1/2 to 1/40 of solar), blue colors ($U-B \sim -0.6$), and intense emission lines (Kunth 1987). In addition, they generally have a relatively high mass fraction in neutral hydrogen (Thuan & Martin 1981), and they are often dominated at optical wavelengths by H II regions (Gordon & Gottesman 1981) that are photoionized by young massive stars (French 1980). Thus, BCDs are noted as a class for their apparent extreme, highly concentrated young population of massive stars but are believed in most cases to harbor an older evolved stellar population as well (Vanzi et al. 1996). UGC 6456 qualifies on all counts (Carozzi, Chamaraux, & Duflot-Augarde 1974; Tully et al. 1981; Fanelli, O'Connell, & Thuan 1988).

Loose & Thuan (1985) were able to distinguish four main classes in a sample of BCDs. They placed UGC 6456 in the largest category, type iE, characterized by one or more irregular, high surface brightness star-forming regions situated near but not coincident with the center of a larger, low surface brightness envelope having elliptical or circular isophotes. For one iE galaxy, Loose & Thuan found that the radial dependence of surface brightness fitted an exponential law outside the star-forming regions.

UGC 6456 has long been considered to be an isolated member of the M81 Group, with a projected distance of about 600 kpc from the major members of the group (see, e.g., Tully et al. 1981). In any case, UGC 6456 is quite isolated; the nearest galaxy (MCG +13-08-059) is about 4.4 distant (4 kpc projected) and appears to be a background elliptical galaxy. It therefore seems unlikely that interaction with other galaxies has played a role in fostering star formation in UGC 6456. Likewise, it seems unlikely that spiral density waves have played a role; Fabry-Perot Hα velocity maps by Thuan, Williams, & Malumuth (1987) show no

[1] Based on observations with the NASA/ESA *Hubble Space Telescope*, obtained at the Space Telescope Science Institute, which is operated by the Association of Universities for Research in Astronomy (AURA), Inc., under NASA contract NAS 5-26555.

[2] The National Optical Astronomy Observatories are operated by AURA, Inc., under cooperative agreement with the National Science Foundation.

TABLE 1

OBSERVATIONS

Filter	Exposure (s)	Gain (e^- DN^{-1})	Images
F656N	800	7	u2pq0501t, u2pq0502t, u2pq0503t
F336W.....	1400	7	u2pq050at, u2pq050bt, u2pq050ct, u2pq050dt
F555W.....	1400	7	u2pq0504t, u2pq0505t, u2pq0506t
F814W.....	1400	7	u2pq0507t, u2pq0508t, u2pq0509t

evidence of rotation and, in fact, little line-of-sight differential motion between the major H II regions, only chaotic motions of order 30 km s^{-1} in the diffuse emission, motions most likely induced by stellar winds from evolving massive stars. Thus, UGC 6456, being one of the nearest galaxies of this type, should afford a good opportunity to disentangle star formation history in a relatively simple dynamical environment.

Using broadband *Hubble Space Telescope* (*HST*) images, we have resolved UGC 6456 into individual stars and have made photometric measurements not only of the young stellar population but of the older underlying stars as well. By means of theoretical models of evolving populations, we have synthesized the color-magnitude diagram for comparison with that which is observed and have drawn conclusions concerning the star formation history of the galaxy.

2. OBSERVATIONS AND DATA REDUCTION

2.1. *HST Images*

UGC 6456 was observed with *HST* and the Wide Field Planetary Camera 2 (WFPC2) on 1995 July 7. Images were obtained through the broadband filters F336W, F555W, and F814W, which approximate the *UVI* photometric bands, and through a narrowband Hα filter, F656N. Multiple frames were obtained through each filter for the purpose of removing cosmic rays; they are listed in Table 1. A mosaic of the four F555W images that constitute the WFPC2 field of view is shown in Figure 1. The central high surface brightness portion of the galaxy was centered in the PC CCD, with some spillover of the galaxy into the WF CCDs. Because of the pattern of the CCDs, a portion of the galaxy to the northeast was not imaged. The PC Hα image is shown in Figure 2 and will be discussed in §§ 2.2 and 6; no Hα emission was detected in the WF fields.

The multiple exposures were averaged with an algorithm designed to remove cosmic rays. A stellar continuum image was constructed from the F555W and F814W images and subtracted from the Hα image to leave pure emission. The emission image was used, in turn, to subtract nebular emission from the three broadband images. Photometry of the stars was performed using the crowded-field photometry software DAOPHOT (Stetson 1987) as implemented in VISTA (Holtzman 1990). The photometry files were purged of hot pixels and residual cosmic rays using the "SHARP" and "CHI" parameters returned by DAOPHOT as a measure of the goodness of fit to the point-spread function, and also by visual examination. The photometry was put on a system relative to Vega using the zero points Z_{syn} given in Table 9 of Holtzman et al. (1995; the calibration and *UBVRI* transformation document for the flight instrumental system) and also transformed to the standard *UVI* system. The stellar photometry is given in Table 2; photometric uncertainties are illustrated in Figure 3.

In order to correct star counts for incompleteness, we added artificial stars to the F555W and F814W images and processed the resulting images in the same way that the original images had been measured. In order not to increase significantly the degree of crowding, we added only 10% of the original luminosity function in each half-magnitude bin. To increase measuring statistics, we added stars to each of the WFPC2 fields in 200 separate experiments. We added the same stars to the F814W image as had been added to the F555W image for different colors: an F555W − F814W of 0.2 for WF images and −0.1 for the PC image to measure the blue side of the color-magnitude diagram (CMD), and an F555W − F814W of 1.1 to measure the red side of the CMD. Because the degree of crowding varied across the field of view of the PC, we separated the stars into three groups: several OB associations, the middle of the galaxy, and the rest of the galaxy. The WF images were assumed to have two degrees of crowding, representing the galaxy and the rest of the field. The percentage incompleteness for these various situations is shown in Figure 4.

2.2. *Additional Ground-based Observations*

We determined the reddening and metallicity of the ionized gas in UGC 6456 from two long-slit emission-line spectra that were obtained for us by P. Massey with the Ritchey-Chrétien spectrograph on the Kitt Peak National

TABLE 2

GALAXY PHOTOMETRY

Star[a]	x[b]	y	F336W	F555W	F814W	F336W − F555W	F555W − F814W
10001.....	981.8	889.8	19.14 ± 0.02	20.04 ± 0.03	19.69 ± 0.02	−0.90 ± 0.03	0.35 ± 0.03
10002.....	984.8	946.4	18.90 ± 0.03	20.14 ± 0.05	20.00 ± 0.02	−1.24 ± 0.05	0.13 ± 0.05
10003.....	991.9	861.3	19.86 ± 0.03	20.33 ± 0.03	20.04 ± 0.02	−0.47 ± 0.04	0.30 ± 0.04
10004.....	831.7	903.8	21.36 ± 0.04	20.95 ± 0.04	20.71 ± 0.02	0.41 ± 0.06	0.24 ± 0.05
10005.....	1018.0	994.7	20.23 ± 0.05	20.97 ± 0.05	21.96 ± 0.06	−0.74 ± 0.07	−0.99 ± 0.08

NOTE.—Table 2 is presented in its entirety in the electronic edition of the Astronomical Journal. A portion is shown here for guidance regarding its form and content.

[a] The first digit of the identification number is the chip number. Within each chip, stars are listed in order of apparent brightness in F555W. There are 22,273 stars in all four chips.

[b] The (x, y) coordinates are those in the F555W image; the coordinate system is indicated in Fig. 1.

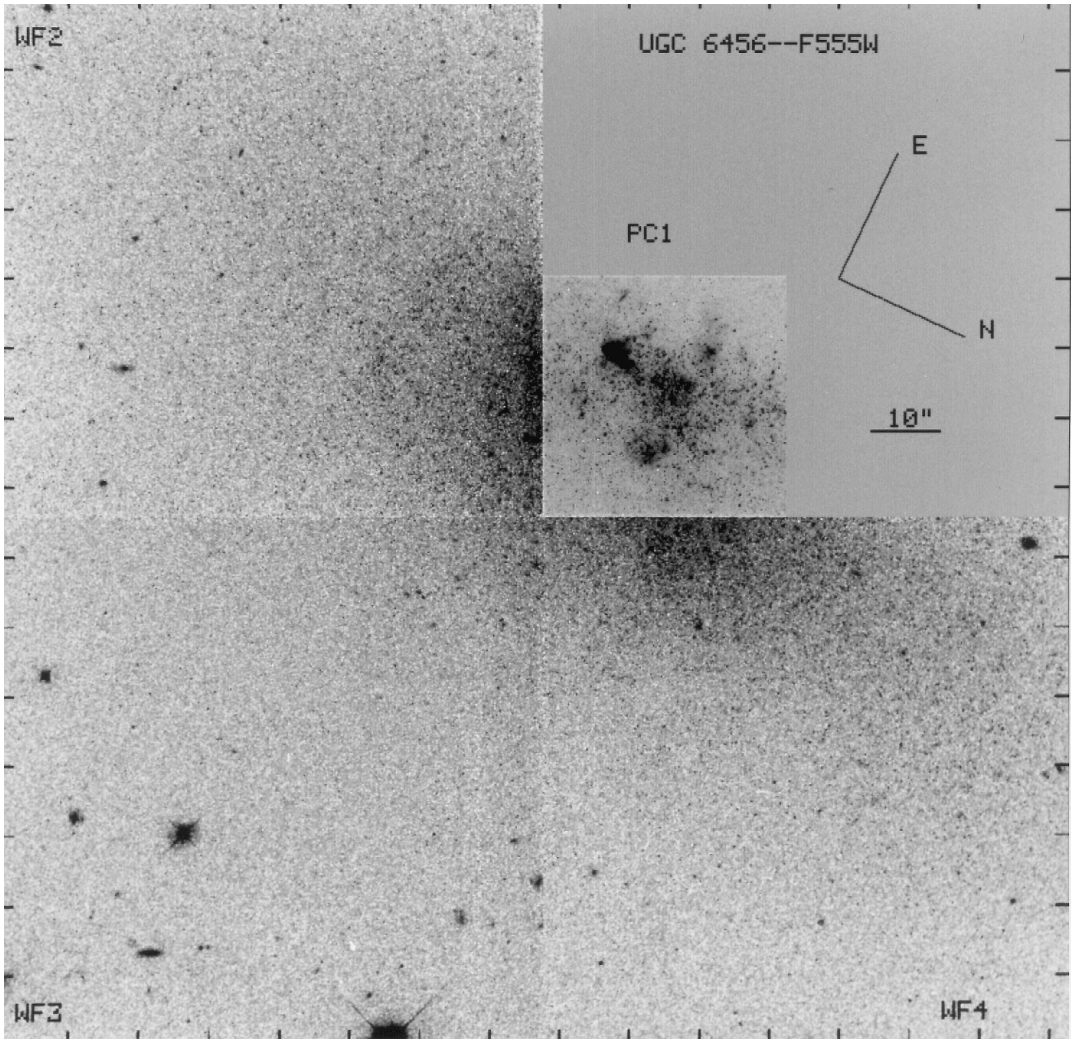

FIG. 1.—Mosaic of the *HST* F555W CCD images. The four CCDs, PC1, WF2, WF3, and WF4, are labeled with their names. North and east are labeled; north is 115° clockwise from the top. The ticks mark the (x, y) coordinate system, marking every 100th pixel beginning with (0, 0) in the bottom left corner. To show spatial detail in PC1, the intensity scaling for PC1 is different than that for WF2, WF3, and WF4.

Observatory 4 m telescope in 1996 October. The slit width was 2″, and the spectra covered the spectral range 3645–5100 Å at a resolution of about 1.8 Å. Referring to the identifications in Figure 2, the slit for one spectrum was centered on H II region 1 at a position angle of 95° and included part of H II region 5. The second slit position crossed H II regions 2, 3, and 4. The Hβ region of both spectra are reproduced in Figure 5. One can readily see the correspondence between the kinematic signature of expanding shells shown by the emission lines and the tendency toward shell-like structure for the H II regions shown in Figure 2. The expansion velocities of the shells are of order 50–70 km s^{-1}.

Emission-line intensities have been measured and the relevant ratios listed in Table 3. The uncertainties given have been computed from the signal-to-noise ratio exhibited by the data. We have derived reddening and metallicities from the data for H II region 1, the brightest of the H II regions crossed by our slits and most typical of the class. Because of underlying stellar absorption, the Hγ-to-Hβ emission ratio

TABLE 3

OBSERVED EMISSION-LINE RATIOS AND DERIVED PROPERTIES

Region	[O II] λ3729/λ3726	[O II]/Hβ	[O III]/Hβ	[O III] λ4363/Hβ	Hγ/Hβ[a]
1	1.39 ± 0.11	0.59 ± 0.02	3.89 ± 0.01	0.064 ± 0.002	(0.44) ± 0.01
1_0[b]	...	0.67 ± 0.02	3.81 ± 0.01	0.067 ± 0.002	...
2	1.43 ± 0.14	2.26 ± 0.11	1.65 ± 0.03	...	0.50 ± 0.01
3	1.50 ± 0.08	1.18 ± 0.03	2.68 ± 0.01	0.049 ± 0.006	0.42 ± 0.01
4	1.37 ± 0.10	1.71 ± 0.06	2.59 ± 0.03	0.063 ± 0.009	0.47 ± 0.01
5	1.80 ± 0.23	2.20 ± 0.12	1.28 ± 0.03	...	(0.51) ± 0.02

NOTE.—[O II] is $\lambda\lambda$(3726 + 3729), and [O III] is λ5007, unless otherwise noted.

[a] For values in parentheses, the emission line was perceptibly sitting in an absorption feature.

[b] The extinction-corrected emission line ratios for region 1 follow the uncorrected values.

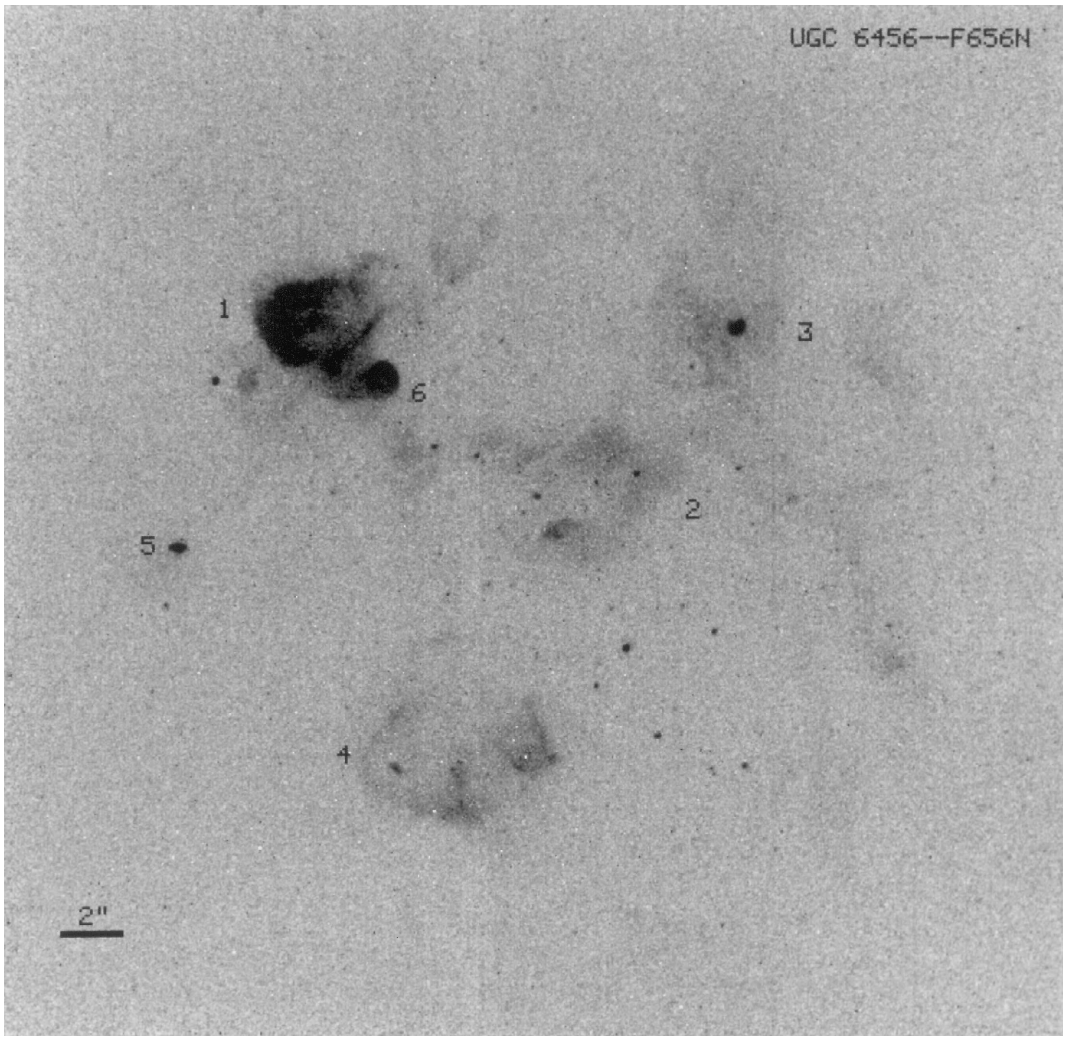

FIG. 2.—*HST* PC image through the F656N filter. The stellar continuum has not been subtracted here. Prominent H II regions are numbered. Orientation is as in Fig. 1.

gives an upper limit to the reddening. From this ratio we determine that $E(B-V) < 0.16 \pm 0.03$ for case B recombination. If underlying stellar absorption contributes 2%, $E(B-V)$ is 0.13; this is what we adopt here. We use the extinction function of Schild (1977). The extinction-corrected emission-line ratios for region 1 are given in Table 3 following the uncorrected values. From the [O III] lines, we determine $T_e = 14000 \pm 200$ K using the method of Seaton (1975), and the ratio of the [O II] lines yields $n_e = 50$ cm^{-3}. The result from the oxygen lines is that O/H is 5.3×10^{-5} and $Z = 0.0014$. The O/H ratio is essentially identical to the value 5.4×10^{-5} determined by Izotov, Thuan, & Lipovetsky (1997). It is also similar to the value 5.8×10^{-5} obtained by Tully et al. (1981) from photographic spectra, but our $E(B-V)$ is significantly different from their value of 0.7. In addition, Tully et al. determined that the reddening function was abnormal in UGC 6456. We believe that the good agreement of our oxygen abundance with that of Tully et al. is the result of chance compensation between their abnormal reddening function and errors in their photographic spectrophotometry.

3. THE COLOR-MAGNITUDE DIAGRAM AND REDDENING

The observed CMDs (F555W magnitude vs. F555W − F814W and F336W − F555W) are shown in Figure 6. The F555W − F814W CMD shows a great abundance of stars populating the red giant branch (RGB), a well-defined asymptotic giant branch (AGB) devolving redward from the top of the RGB, a blue plume of hot stars ranging from luminous supergiants to main-sequence stars, and a red plume of luminous supergiants. If we assume that the bright limit of red giants is at $M_I = -5$ (F814W = 23.25 for the distance modulus determined in § 4), the red giant stellar population contributes about a factor of 3 more light in the I band than do the red supergiants. Thus, in this galaxy it is the older stellar population that is dominating the red light, rather than the young evolving massive stars.

Foreground reddening to UGC 6456 is small, $E(B-V) = 0.02$, according to Burstein & Heiles (1984). Very different estimates of the total reddening to UGC 6456 are found in the literature. From photographic spectra Tully et al. (1981) found an $E(B-V)$ of 0.7 with a peculiar wavelength dependence, while Fanelli et al. (1988) used a value of 0.08 in the analysis of ultraviolet observations. The latter value is consistent with the amount of extinction usually found in irregular-type galaxies and with the value of 0.13 that we measured for H II region 1 in UGC 6456. We have also found that the bulk of the stars are consistent with an $E(B-V)$ of about 0.04 and an $R_V = A_V/E(B-V)$ of 3.1. That this is reasonable can be seen in the color-color

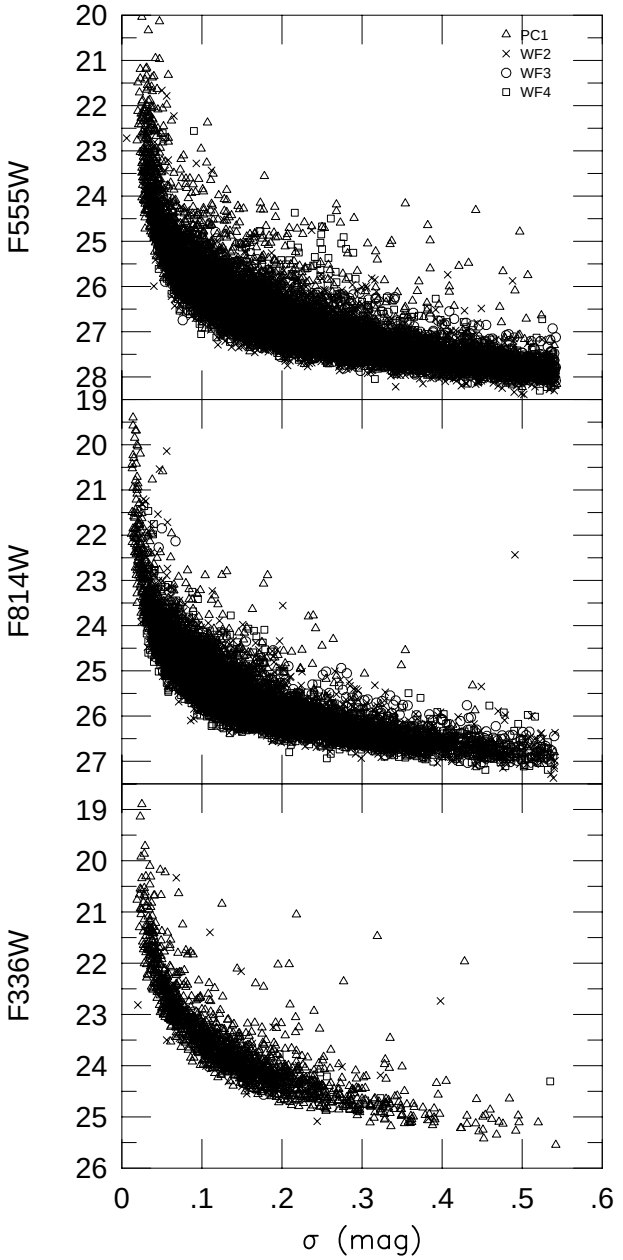

FIG. 3.—Uncertainties in the stellar photometry for each filter. The uncertainty includes both photon statistics and a measure of the goodness of fit by the point-spread function. Photometry from the four CCDs are distinguished with different symbols as shown.

diagram shown in Figure 7. However, when we examine in § 6 the CMDs of two stellar associations separately, we find more reddening for the stars associated with H II region 1. Because these young stellar associations are surrounded by emission nebulosity, it is reasonable that they should show more reddening and extinction. The associations are defined below, but we mention here that we have determined an $E(B-V)$ of 0.08 for association 1 and 0.06 for association 5. All other stars were assumed to suffer extinction corresponding to a total $E(B-V)$ of 0.04, which corresponds to extinctions in F336W, F555W, and F814W of 0.18, 0.12, and 0.08, respectively (Holtzman et al. 1995).

4. DETERMINING THE DISTANCE

UGC 6456 has long been assumed to be a member of the M81 Group, but its distance has never been measured directly. With the measurement of a well-developed RGB, we are in a position to use the tip of the RGB to determine the distance. We have used the method outlined by Lee, Freedman, & Madore (1993), in which the tip of the RGB is taken to be represented by a break in the slope of the I-band luminosity function. For this purpose we converted the extinction-corrected F814W data to I using the transformations given by Holtzman et al. (1995) and corrected the counts for incompleteness using the measurements shown in Figure 4. The luminosity function is shown in Figure 8, where we have marked our choice for the break in the slope at an I magnitude of 24.25. In Figure 8, we show the luminosity function with a binning of 0.1 mag. However, we also explored the use of 0.2 and 0.3 mag bins and found no change in where we chose the break. Because brighter, younger stars in a mixed-age population can potentially confuse the tip of the RGB, we also experimented with excluding the stars in the PC image, where the bulk of the young stars are found. Again, the same I magnitude for the break was found.

We took the $(V-I)_0$ color of the tip of the RGB to be 1.41, which gives a bolometric correction BC_I of 0.54 according to Lee et al. (1993). The bolometric magnitude of the tip of the RGB, $M_{\rm bol,TRGB}$, is determined from [Fe/H], which in turn is determined from the color of the RGB at $M_I = -3.5$. We determined [Fe/H] to be -1.85 and $M_{\rm bol,TRGB}$ to be -3.46. Therefore, M_I for the tip of the RGB is -4.00, and the distance modulus $m - M = 28.25 \pm 0.10$, where the uncertainty is our uncertainty in the location of the change of slope in the luminosity function. This distance modulus agrees to within the uncertainties with the value 28.4 found by Schulte-Ladbeck, Crone, & Hopp (1998) from our data and corresponds to a distance of 4.5 ± 0.2 Mpc, substantially greater than the 3.2 Mpc that had been assumed for the galaxy as a member of the M81 Group. The consequence of this distance determination is shown in Figure 9, where our extinction-corrected photometry is superposed on the globular cluster sequences of Da Costa & Armandroff (1990).

Unfortunately, the determination of the distance by this method is not entirely unambiguous. Although a few galaxies for which distances have been determined by both Cepheids and the tip of the RGB have yielded comforting agreement (see, e.g., Sakai, Madore, & Freedman 1996 in the case of Sextans A), there is reason to doubt that the tip of the RGB is always reliable in a mixed-age population. Young massive stars of order 3 $M_\odot$ that become red supergiants can mingle with older, lower mass stars just above the tip of the RGB, confusing this region of the CMD. This is seen in the analysis of the CMD of the galaxy NGC 5253 by Saha et al. (1995). They find that the tip of the RGB in that galaxy is defined by stars only about 100 Myr old. This problem could be particularly acute for a galaxy in which the star formation rate fluctuates wildly, as could be the case for a BCD such as UGC 6456, and should be borne in mind as we compare our photometry with theoretical models. In any case, we adopt a distance modulus of 28.25 for all subsequent discussion.

5. SPATIAL DISTRIBUTIONS

On our images of UGC 6456 the bluest and youngest stars are largely confined to the field of the PC, where they exhibit a clear tendency for clustering, whereas the popu-

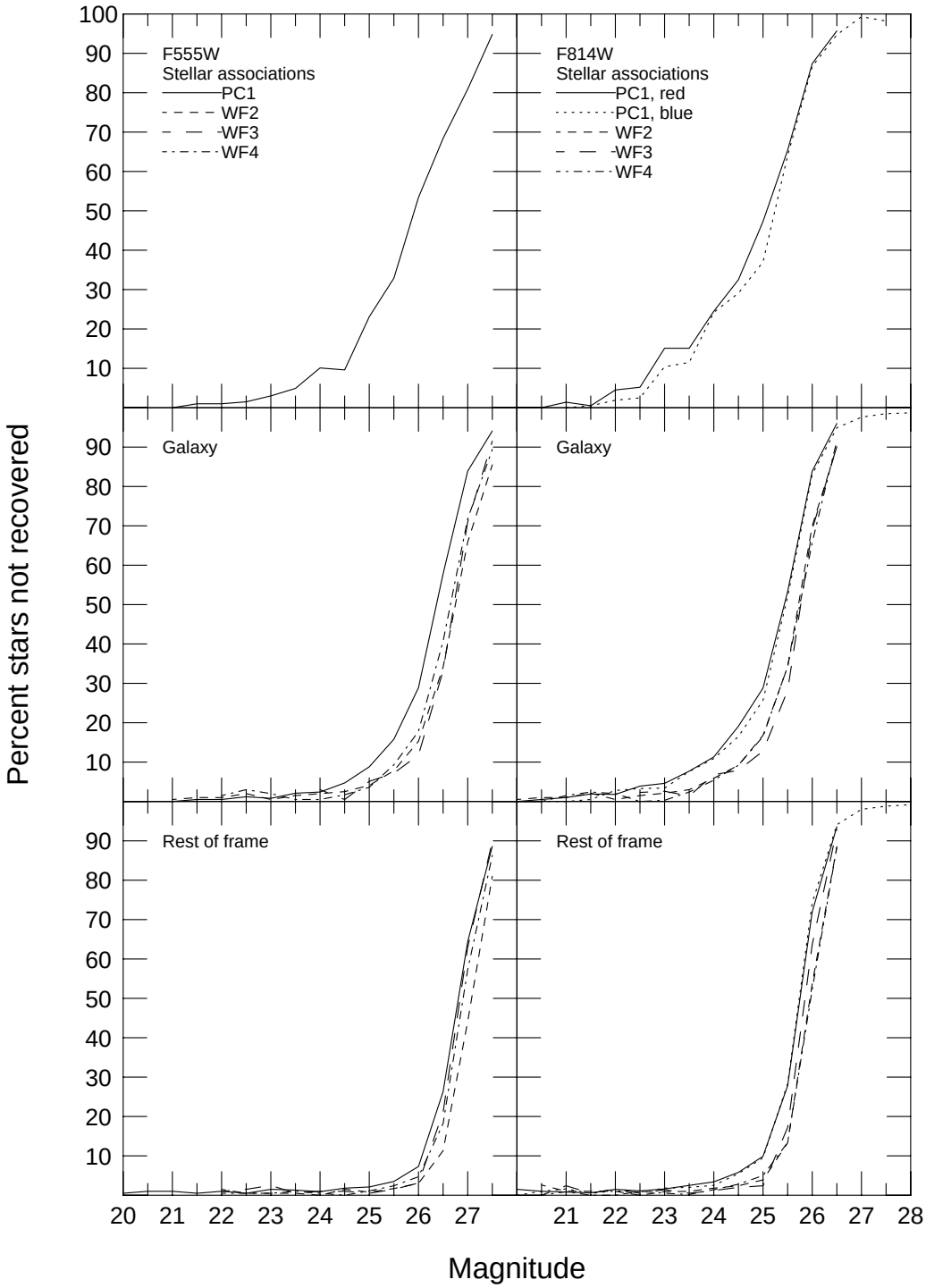

FIG. 4.—Percentage incompleteness as a function of magnitude for each of the CCDs and the different regions within each CCD field of view. F555W is shown on the left and F814W on the right. For PC1 both the blue and red F814W incompleteness factors are shown; for the WF CCDs only the red is shown.

lation of giants spills over into the WF fields, especially WF2 and WF4. When viewing our images in color, one gains the impression that the luminous stars, especially the red supergiants, are not strongly associated with the clustering shown by the bluer, less luminous stars. The effect is easily seen in the two-point correlation functions. Even so, the young stars all tend to be situated in the central region of a more extended, roughly elliptical distribution of stars that are more evolved.

In order to study the character of the underlying galaxy defined by the evolved population, a densely populated region of the RGB was selected, bounded by $1.0 < \mathrm{F555W} - \mathrm{F814W} < 1.6$ and $24.5 < \mathrm{F814W} < 26.0$. The average surface density of stars was determined in each of a 4×4 matrix of identical rectangular regions for each of the four WFPC2 fields. We assumed that the distribution of stars can be represented by a homologous sequence of isodensity contours identical in eccentricity, orientation, and center, with the semimajor axes defined by the centers of gravity for the stars in the regions. Finally, we optimized eccentricity, orientation, and center by maximizing the correlation coefficient in the relationship between semimajor axis and the

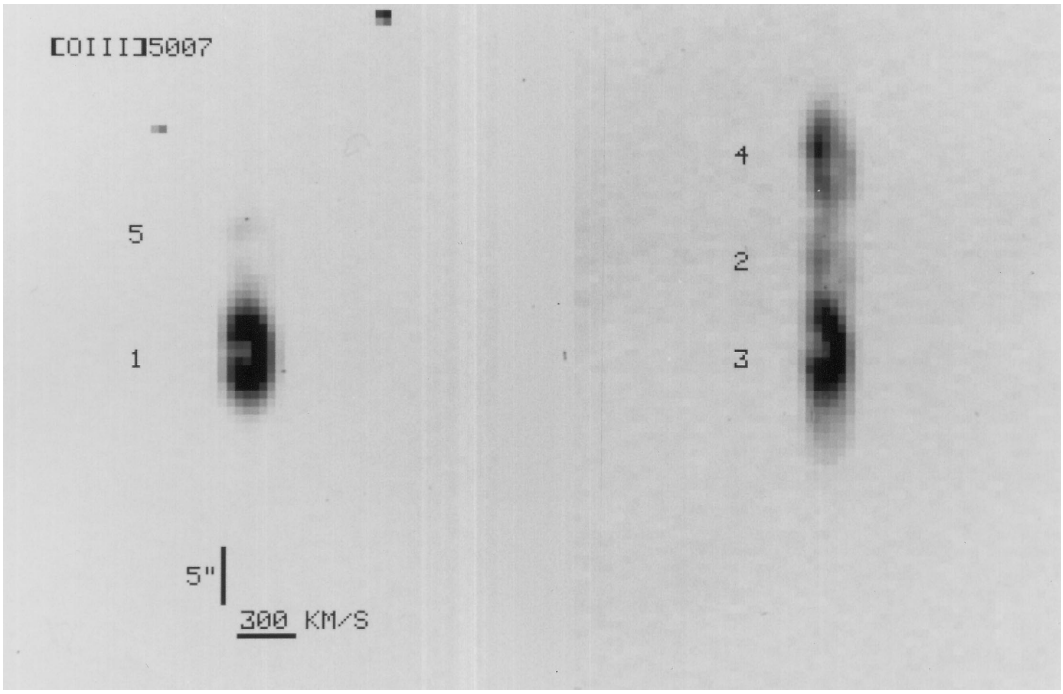

FIG. 5.—Hβ emission line from our two long-slit spectra are displayed to show the line splitting that is the signature of an expanding shell

logarithm of surface density. The final parameters are an eccentricity of 2.425, a position angle for the major axis at 168° (about 53° counterclockwise from the vertical in Fig. 1), and the center at $x = 940$, $y = 830$. For comparison with the latter, the centroid of the young stars is at about the same x-value but is about 100 WF pixels greater in y, that is, more nearly centered in the PC field.

Figure 10 is a plot of the relationship between the natural logarithm of surface density and semimajor axis as determined. The relationship is seen to be essentially linear, so that the falloff in the surface density of evolved stars is exponential. A least-squares straight-line fit to the points in Figure 10 yields a slope of -2.36×10^{-3}, or a $(1/e)$th semimajor axis of 424 WF pixels, 42".4, or about 1 kpc. This is well within the range of scale lengths determined by Papaderos et al. (1996) for a sample of BCDs. UGC 6456 is clearly not a young galaxy; it is a galaxy of evolved stars that have at least partially relaxed into a smooth distribu-

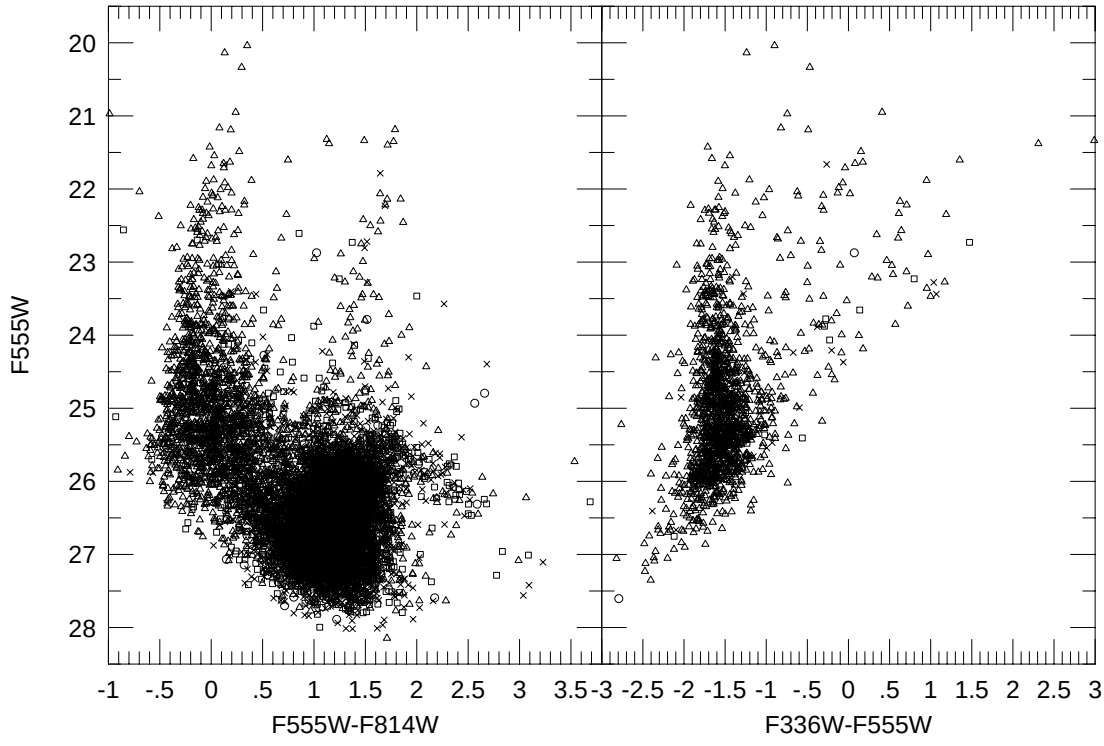

FIG. 6.—Color-magnitude diagrams for all the stars in the galaxy: F555W − F814W (*left*) and F336W − F555W (*right*). Symbols are the same as in Fig. 3.

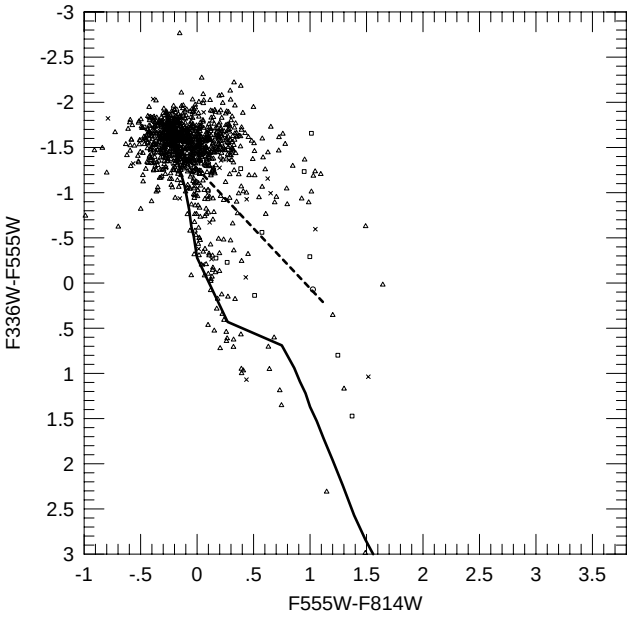

FIG. 7.—Color-color diagram for all of the stars in the galaxy. Symbols are the same as in Fig. 3.

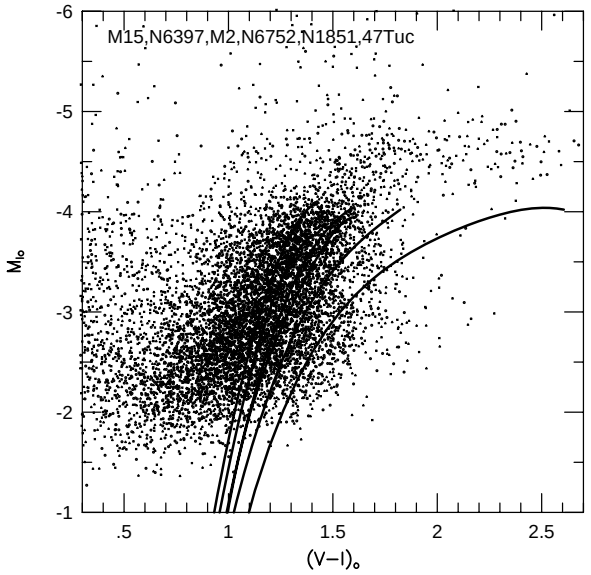

FIG. 9.—Red giant branch and AGB of the galaxy color-magnitude diagram. Superposed are observed globular cluster sequences from Da Costa & Armandroff (1990). The approximate metallicities for the six clusters are in the order listed, beginning with M15: $Z = 0.0001$, 0.0002, 0.0004, 0.0005, 0.001, and 0.003.

tion of unremarkable character. Were it not for the highly luminous contribution from recent star formation events scattered about the inner region, it would probably be classified as a dwarf elliptical galaxy. A discussion of other relationships between the distribution of stars in the CMD and in space will be deferred to a later paper.

6. STELLAR ASSOCIATIONS AND THE CURRENT STAR FORMATION ACTIVITY

UGC 6456 is seen to harbor a centrally located cloud of young stars, mostly confined to the PC, within which there are surface density fluctuations that in some cases invite identification as clusters or associations. Six such groupings are identified in Figure 11, a reproduction of the F555W PC field. There are two large associations, Nos. 1 and 5; associations 2, 3, 4, and 6 are sparse, containing only 12, 3, 9, and 4 luminous blue stars, respectively. These latter associations resemble small OB associations seen in nearby galaxies and will not be discussed further. However, the larger OB associations, Nos. 1 and 5, merit a more detailed discussion.

6.1. *Association 1*

The CMD for the large southern OB association (1) is

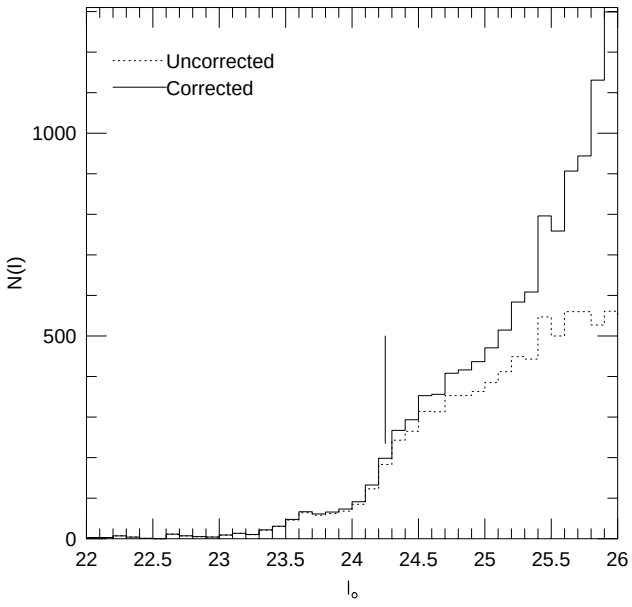

FIG. 8.—*I*-band luminosity function for the stars in UGC 6456. The function is shown uncorrected and corrected for incompleteness in the star counts as determined from artificial-star experiments. The luminosity function with 0.1 mag bins is shown. The choice of the tip of the RGB is shown as a solid vertical line.

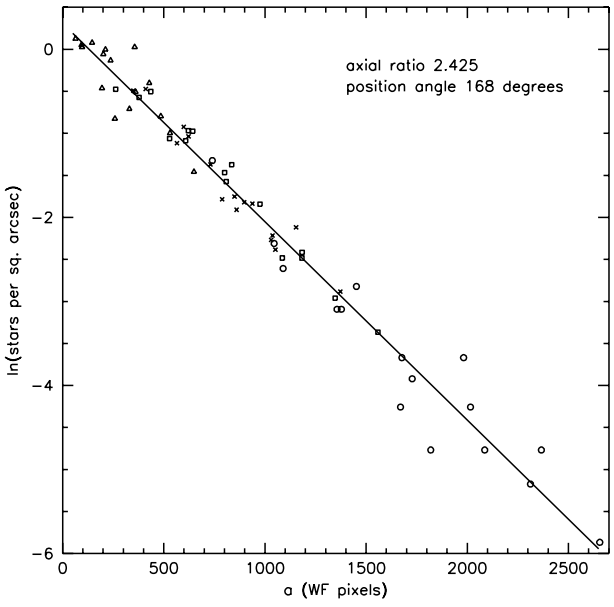

FIG. 10.—Natural logarithm of surface densities plotted vs. the semimajor axes (in WF pixels) of ellipses assumed to have identical eccentricity, orientation, and center. The average surface density of stars was determined in each of 16 (x, y) bins in each WFPC2 field defined by dividing each field into a 4×4 matrix of identical rectangular regions.

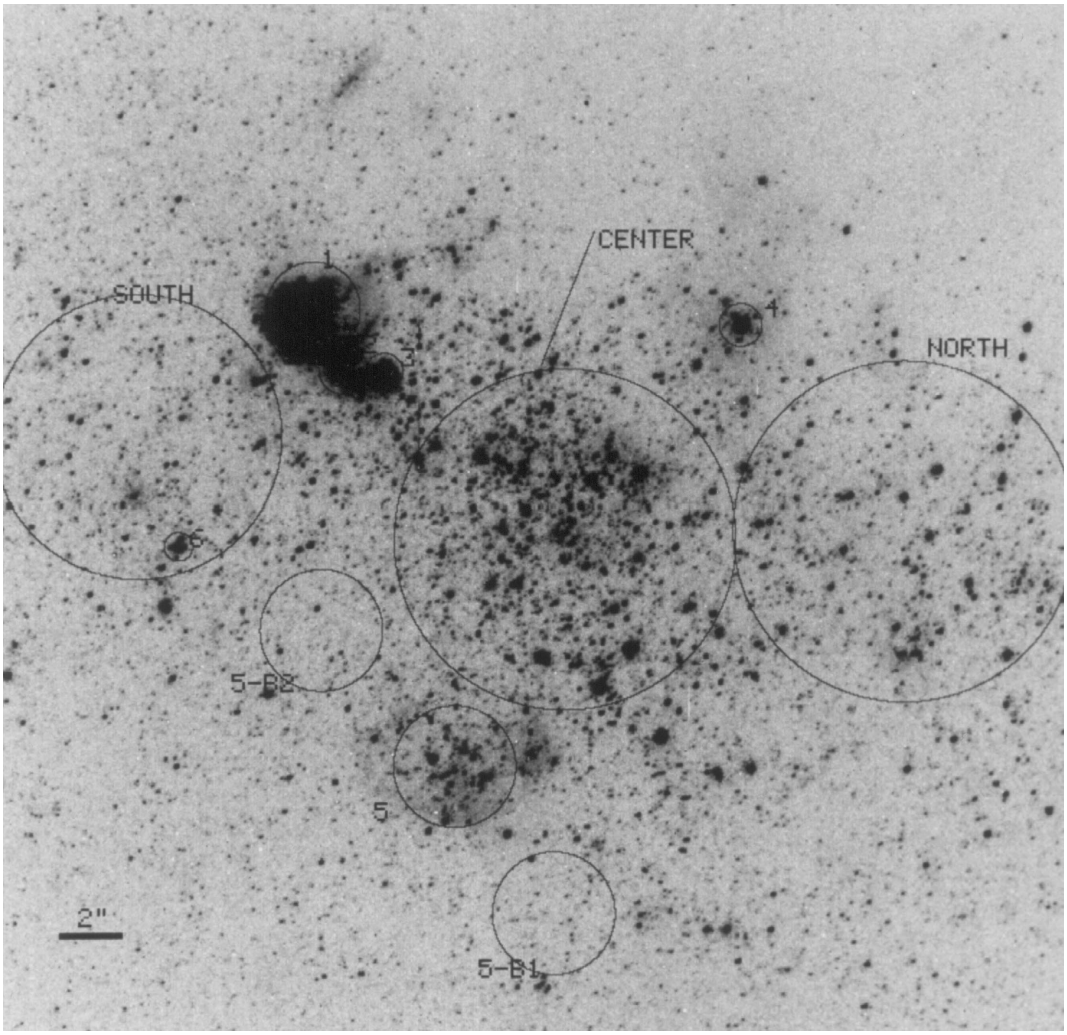

FIG. 11.—Regions considered separately in the text are outlined on the F555W PC image and stellar associations are numbered. "5-B1" and "5-B2" are regions used to determine the underlying galactic background for association 5.

shown in Figure 12. It contains 25 blue stars with $M_{F555W,0}$ brighter than -4, and 27 stars when corrected for incompleteness. These are likely to be O stars in the cluster. There are two bright red stars that fall within the magnitude range expected to be occupied by red supergiants of class Ib. The other, fainter red stars are probably red giants in the underlying population of evolved stars. In terms of numbers of luminous stars, this association is typical of OB associations, which can contain anywhere from tens to hundreds of luminous stars.

In Figure 12, we compare isochrones with the data. These isochrones are those constructed by Holtzman et al. (1995) and used by Hunter et al. (1995) in the analysis of the R136 cluster in the Large Magellanic Cloud. The number of stars is small, but it appears that an age of 4–5 Myr is appropriate. This age is comparable to that of NGC 604 in M33.

Hunter (1995) and Hunter et al. (1996) have summarized the spatial density of luminous blue stars formed in various types of star-forming regions. By comparison with other OB associations, R136, the luminous compact star cluster in the Large Magellanic Cloud, has a density 100–300 times greater; the cluster associated with NGC 604, the giant H II region in M33, is about normal; and NGC 206, the giant OB association in M31, is sparser. Association 1 in UGC 6456 presents a surface density of 0.003 luminous stars pc^{-2}. This is one-seventh of the value for NGC 604 and other OB associations and 1/600 that of R136. Thus, association 1 is a little less concentrated than what we would take to be "normal."

We cannot determine a stellar initial mass function (IMF) for the stars in association 1, because we have only detected the massive stars, stars for which spectral classification is required for the determination of a reliable IMF (Massey et al. 1995). It is also dangerous to compare luminosity functions because the massive stars evolve so quickly. However, keeping this in mind, we have calculated the slope of the main-sequence luminosity function (log number of stars vs. $M_{F555W,0}$) for association 1 and find it to be 0.37 ± 0.09 for stars having $M_{F555W,0}$ in the range -5 to -7. This compares well with the luminosity function slope 0.44 ± 0.08 for NGC 604 in the same luminosity range.

Association 1 is encircled by a partial shell of Hα emission that is open to the northeast and higher in surface brightness on the opposite side. Using a ground-based Hα image, we measure the extinction-corrected Hα luminosity in this shell to be 5×10^{50} photons s^{-1}. For an ionizing flux per star determined for a Salpeter-weighted stellar IMF (a rough estimate), the 27 stars within the association would

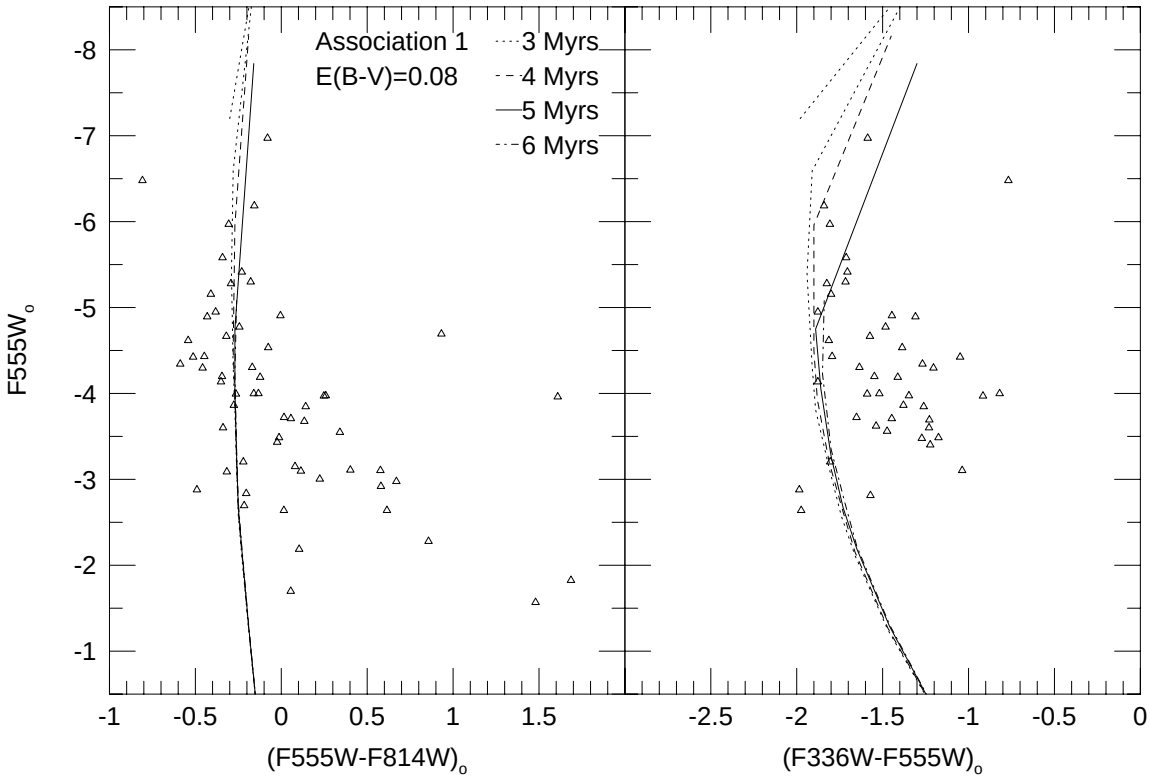

FIG. 12.—Color-magnitude diagrams for stars in the stellar association numbered 1 in Fig. 11: F555W − F814W (*left*) and F336W − F555W (*right*). An $E(B-V) = 0.08$ was used. Isochrones are those constructed by Holtzman et al. (1995) as implemented for the R136 cluster in the Large Magellanic Cloud by Hunter et al. (1995).

be expected to produce about 5×10^{50} photons s^{-1}, in agreement with the photon rate required to produce the nebulosity.

The shell itself has a radius of 79 pc measured from the center of the stellar association, and our long-slit spectra suggest a velocity of expansion of $\sim$65 km s^{-1}. According to the shell production models of McCray & Kafatos (1987), the encircled stellar population could produce a shell of that radius in about 1 Myr. This is a younger age than the 4–5 Myr suggested by the isochrones. If the age of 4–5 Myr is correct, this could suggest that star formation in this region was not instantaneous (Shull & Saken 1995).

6.2. *Association 5*

Association 5 is also located in an Hα shell, although one that is much more diffuse than that which encircles association 1. The ionization rate of the gas is 2.8×10^{50} photons s^{-1}, corrected for extinction. The CMD is shown in Figure 13. We also examined the stellar population of two nearby regions of the same size (5-B1 and 5-B2 in Fig. 11) in order to estimate the background contribution. After correction for this contribution and incompleteness, we count 28 stars in association 5 more luminous than $M_{\mathrm{F555W},0}$ of -4. These are blue main-sequence and supergiant stars. There are no likely red supergiant candidates. From a comparison with isochrones, the association could be 5–6 Myr old. The spatial density of luminous stars is about half that of association 1, and the stars produce roughly 60% more photons per second than are being used to ionize the surrounding gas. According to the models of McCray & Kafatos (1987) and Weaver et al. (1977), the shell of radius 100 pc and expansion velocity 65 km s^{-1} could be produced by this association in about 1 Myr. Just as in the case of association 1, the shell expansion models and isochrones disagree on predicted ages for the region, suggesting a more complex history than the models assume.

6.3. *Sizes and Ages of Star-forming Units*

We have made the point that the star-forming units identified as associations 1 and 5 are modest in scale compared with examples of truly aggressive star formation activity known in other galaxies. Units identified as 2, 3, 4, and 6 are even smaller. Nevertheless, all six bear an unmistakable geometric relationship with the H II regions shown in Figure 2. There is also Hα emission in other regions as well, particularly in the larger association labeled "center" in Figure 11. The CMD for stars included within the 240 pc diameter circle is shown in Figure 14. A comparison with the superposed isochrones suggests that this is a mixed-age population with a subpopulation of blue supergiants that could be as young as 5 Myr superposed on an older population 10 Myr or more in age. The presence of approximately 20 red supergiants is in accord with the existence of a more evolved population of about that age.

Luminous blue stars are found throughout most of the PC field. The regions identified in Figure 11 as "north" and "south" also contain stars compatible with ages of 5 Myr and 10 Myr or more. In fact, even if we exclude all stars lying within all regions outlined in Figure 11, the remaining stars still suggest a range of ages from 5 to 10 Myr, or even older. Within an F555W magnitude range of 22 to 23, the color distribution is bimodal with one peak corresponding to the 5 Myr age and another, stronger peak about a quarter of a magnitude to the red. Thus, we seem to be

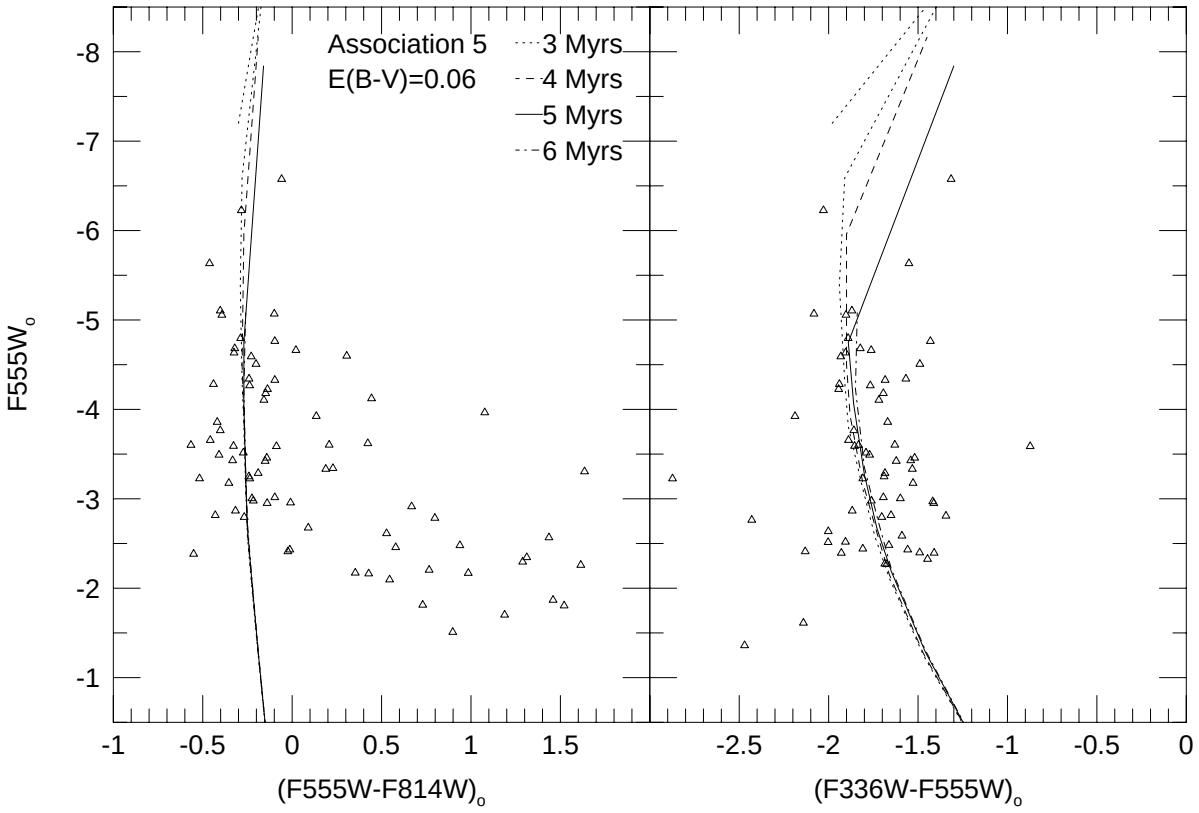

FIG. 13.—Color-magnitude diagrams for stars in the stellar association numbered 5 in Fig. 11: F555W − F814W (*left*) and F336W − F555W (*right*). An $E(B-V) = 0.06$ was used. Isochrones are those constructed by Holtzman et al. (1995) as implemented for the R136 cluster in the Large Magellanic Cloud by Hunter et al. (1995).

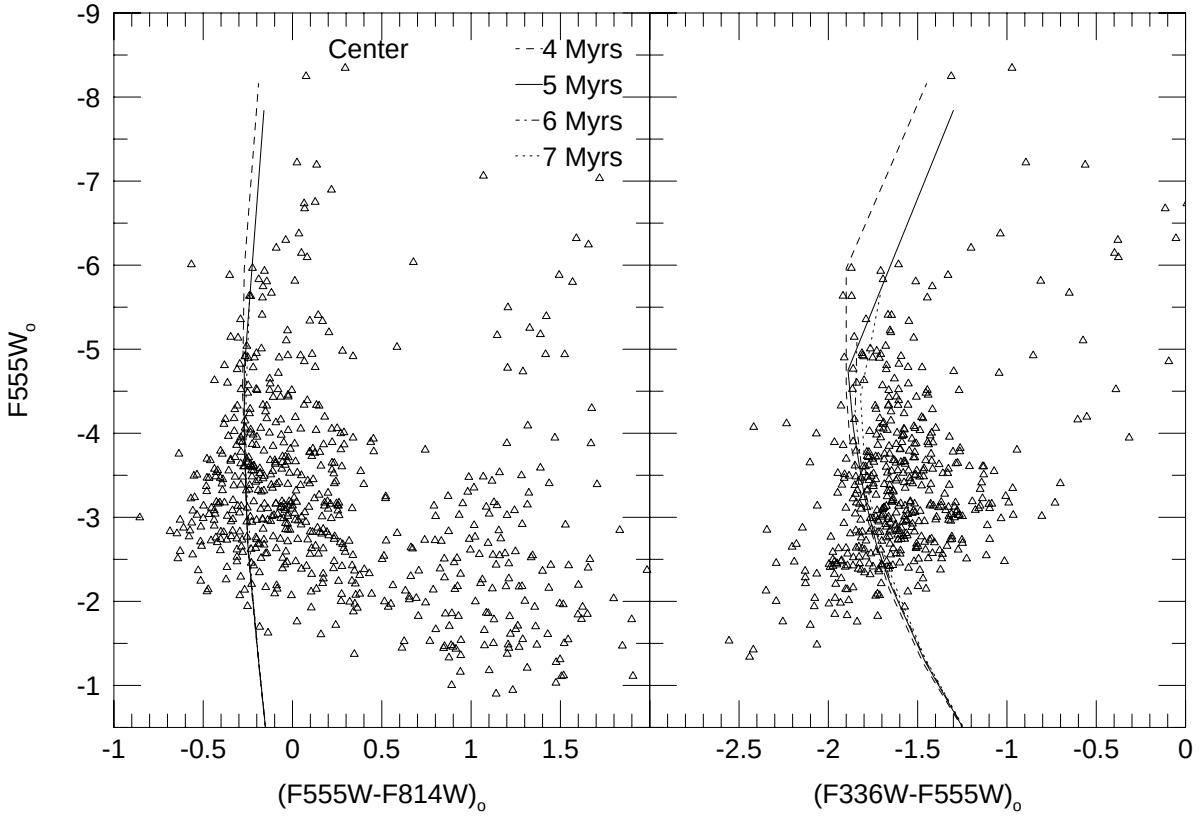

FIG. 14.—Color-magnitude diagrams for stars in the central 240 pc of the galaxy, identified in Fig. 11: F555W − F814W (*left*) and F336W − F555W (*right*). Isochrones are those constructed by Holtzman et al. (1995) as implemented for the R136 cluster in the Large Magellanic Cloud by Hunter et al. (1995).

seeing a spatial and temporal superposition of star-forming events, the most recent of which are in many cases clearly associated with H II regions that overlie or interpenetrate a background of slightly older stars that is less well delineated but perhaps defined by the distribution of red supergiants.

7. MODELING THE COLOR-MAGNITUDE DIAGRAM

In experimenting with models to simulate the CMD we have used the technique of Tolstoy & Saha (1996). Model CMDs are constructed through Monte Carlo simulations using theoretical stellar evolution tracks (a technique pioneered by Tosi, Greggio, & Focardi 1991). The models are compared with the data quantitatively to determine which model best reproduces the distribution and relative numbers of stars in the CMD. The likelihood of a model matching the observed CMD is determined using Bayesian inference. Thus, the CMD can be matched to different models quantitatively, and the best match can be chosen in a consistent way.

7.1. *The AGB Population and Related Matters*

UGC 6456 joins the very small list of galaxies in which a well-defined AGB has been unambiguously detected. This feature is seen at F555W − F814W > 1.8 in Figure 6 and at $(V-I)_0 > 1.6$ in Figure 15. Among irregular galaxies, AGB stars have been seen in small numbers in IC 1613 (Freedman 1988) and LGS 3 (Lee 1995), and a well-populated AGB sequence is observed in NGC 6822 (Gallart et al. 1994).

AGB stars can be informative as tracers of stellar populations older than ~0.25 Gyr and more metal-rich than $Z \sim 0.001$. Much can be learned about age at known metallicity and about metallicity at known age, but there can be considerable ambiguity if neither age nor metallicity can be constrained. The dilemma can be particularly acute when confronted with a mixed population where we expect an inverse relationship between metallicity and age as in a normal chemical enrichment scenario. This is because AGB stars become bluer and more luminous with both decreasing age and decreasing metal abundance. This is illustrated in Figure 15, where we have reproduced our CMD with superposed isochrones from Bertelli et al. (1994) for two metallicities and four ages.

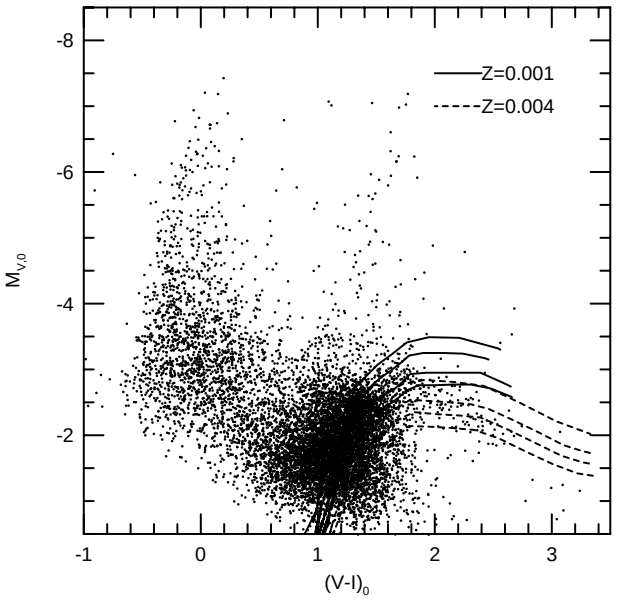

FIG. 15.—AGB isochrones from Bertelli et al. (1994) shown superposed on the observed CMD of UGC 6456. The isochrones for two metallicities, $Z = 0.001$ and $Z = 0.004$, are shown. For each metallicity the isochrones are for populations of ages 1.3, 2, 3, and 5 Gyr, with the youngest isochrone being the brightest.

In Figure 15, it is seen that the redward extent of the AGB stars is consistent with the $Z = 0.001$ isochrones but that they appear too faint by 0.5–0.75 mag and fall a little short of a perfect fit to the shape of the isochrones. By comparison, the stars match the luminosity and better fit the shape of the $Z = 0.004$ isochrones but fall short in extension to the red. However, in making a choice of metallicity there are several circumstances that must be considered.

First of all, although the isochrones for $Z = 0.004$ seem to be a better match to the luminosity of the AGB stars than do those for $Z = 0.001$, we confess to a degree of reluctance in supposing the AGB population to have a metallicity higher than that which we have determined for the gas in the H II regions. And even though it is by no means impossible that the metallicity of the gas could be out of step with a progressive enrichment scenario, it would not be our first choice. However, it is clear from Figure 15 that an adequate match between the luminosity of our AGB stars and the $Z = 0.001$ isochrones would require an increase in our distance estimate by at least 0.5 in distance modulus. Although in § 4 we made reference to potential problems in estimating distance from the apparent brightness of the tip of the RGB, we find that we have no direct evidence upon which to base the requisite revision.

There may be some risk in taking the isochrones at face value. Although the qualitative relationships between the isochrones are in accord with physical expectation, we see evidence that they are quantitatively flawed. At least, they do not agree with the globular cluster sequences of Da Costa & Armandroff illustrated in Figure 9. They are too blue and too bright. For example, the Bertelli et al. isochrone for $Z = 0.0004$ and an age of 15 Gyr falls far to the left of the RGB sequence for M2 at the same metallicity and even to the left of M15 at a metallicity of 0.0001. We will also find from our modeling of the RGB using evolutionary tracks that there is a similar discrepancy at $Z = 0.001$.

Referring again to Figure 9, where we compare our absolute photometry with globular cluster sequences, we see that the color at the top of the RGB compares well with the NGC 6397 sequence, for which Da Costa & Armandroff quote a metallicity of $Z = 0.0002$. At such a low metal abundance a population cannot have such a well-developed AGB; also, in order for a higher metallicity population to have the observed color at the tip of the RGB, it would need to be substantially younger than the globular cluster populations. We also see that the RGB siblings of the AGB stars would tend to obfuscate any evidence of a low-metallicity RGB.

Thus, it seems to us most likely that the AGB population was preceded by an earlier, low-metallicity population that provided the chemical enrichment for the later population. For such an isolated galaxy, the only alternative sources for such enrichment would be more "cosmological" in nature and highly speculative. We therefore assume that an earlier population is present and that its RGB is blended with that of the later AGB population in such a way as to be difficult to distinguish on the basis of the photometric data alone.

In view of the uncertainties reflected in the foregoing considerations, we have elected to simulate the CMD only for a $Z = 0.001$ population at the distance determined in § 4. An additional influence on our modeling is the fact that evolutionary tracks are not available for AGB stars. This means that number densities of stars along tracks and how these might correlate with a past star formation rate are not known. We have, therefore, modeled only the stars blueward of the solid line in Figure 16, eliminating the majority of the AGB stars. We recognize that this attempt at exclusion will probably not be entirely successful in the event that we are dealing with mixed-age and mixed-metallicity populations.

7.2. *Modeling the RGB*

Figure 17 shows $Z = 0.001$ stellar evolutionary tracks from Schaller et al. (1992) and $Z = 0.004$ tracks from Charbonnel et al. (1993). The evolutionary models have been convolved with Kurucz (1991) model atmospheres to put them on the VI photometric system. A comparison of the tracks with the data suggests that there is no strong evidence for a large spread in metallicity within the galaxy and that the $Z = 0.001$ tracks provide a somewhat better match to the data. Therefore, we use only the $Z = 0.001$ evolutionary tracks in modeling the CMD. We also assume a Salpeter (1955) stellar IMF for stars from 0.1 to 100 $M_{\odot}$. Our numbers of stars formed as a function of time are relative; we will discuss absolute rates in a subsequent section.

We begin by analyzing the most populous part of the CMD, the RGB. As can be seen in Figure 16, the shape of the RGB is qualitatively similar in all of the CCDs. We capitalize on this by modeling the photometry in the WF2 field first to examine the older stellar population. In this way we can determine the age constraints on this population independent of the young stars that pervade the PC field, where the center of the galaxy is imaged.

We have created a series of models in 50 Myr intervals over the age range 400–2000 Myr; these are shown in Figure 18. Using the algorithm described by Tolstoy & Saha (1996), we have determined the best mixture of these models in fitting the observed CMD—a mixture that defines the most likely star formation history. As we have said, such a determination using the RGB may be limited by the confusion of the RGB by AGB stars. This series of experiments has also illustrated another limitation inherent in using the RGB for determining star formation history, to

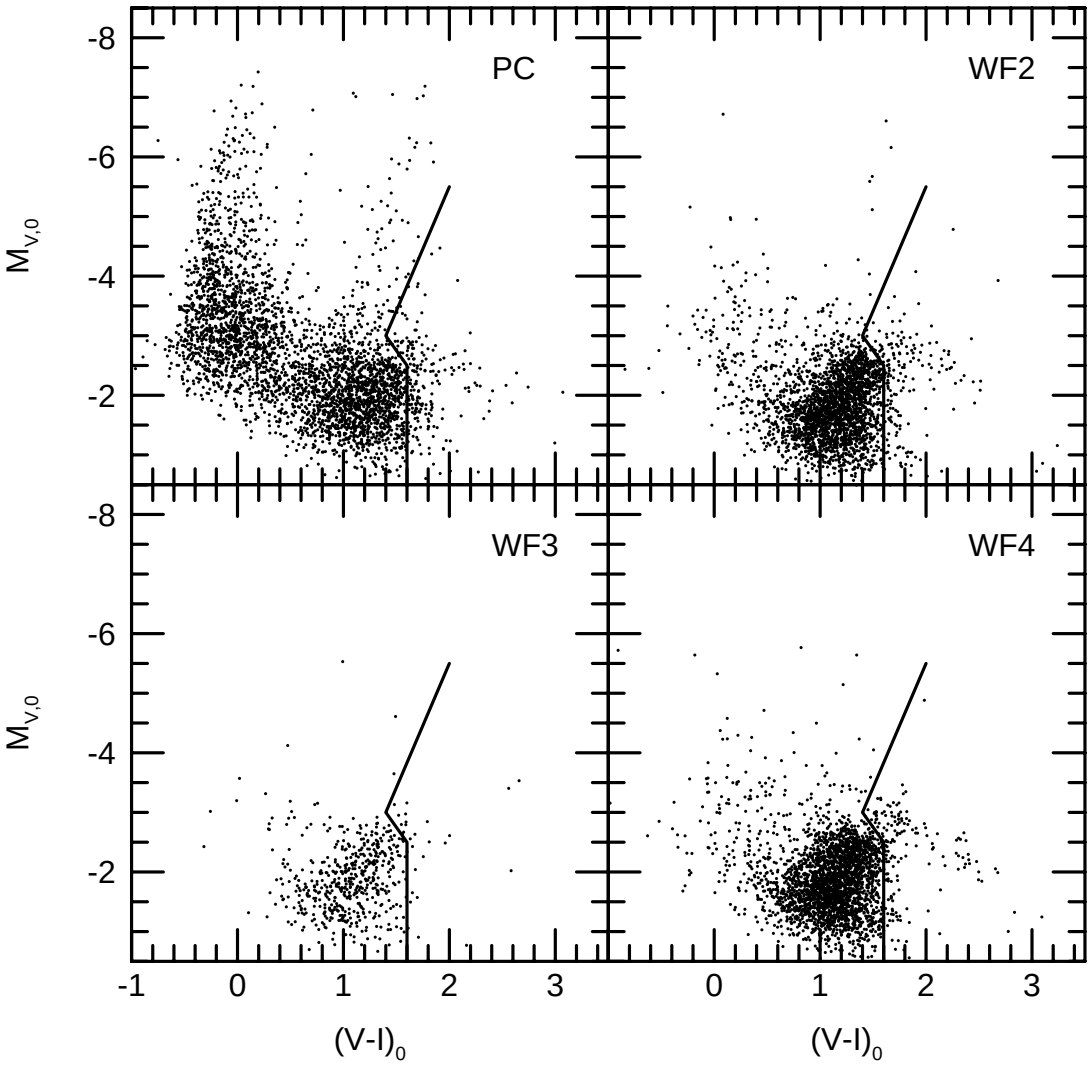

FIG. 16.—Observed color-magnitude diagrams shown for each WFPC2 CCD separately. Overplotted is an identical line that demarks the region to the redward of which exclusively contains AGB stars. The line helps to guide the eye in comparing the RGB between the different CCDs.

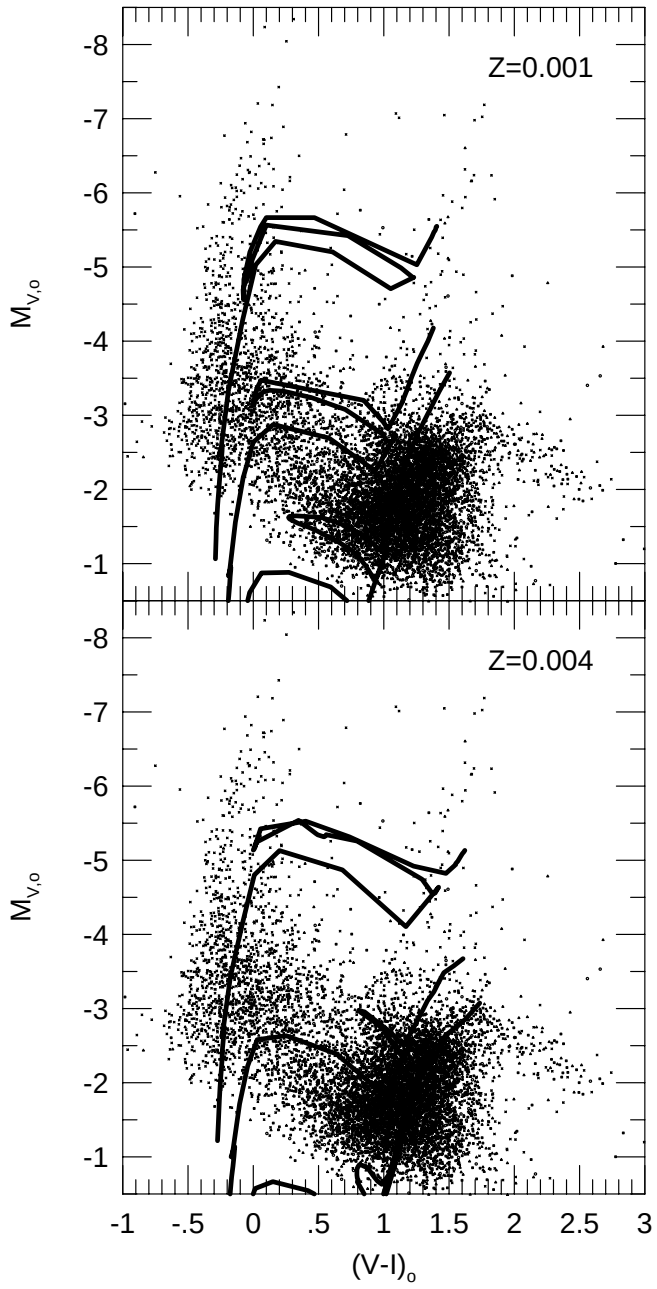

FIG. 17.—Observed color-magnitude diagram with the stellar evolution tracks (Schaller et al. 1992; Charbonnel et al. 1993) superposed for two metallicities and stellar masses 3, 5, and 10 $M_\odot$.

wit, stars evolve slowly through this region. Beyond 800 Myr the structure of the CMD varies very slowly with time. The RGB, therefore, is most sensitive to star formation back to about 800 Myr. For ages 1–1.2 Gyr, the part of the CMD that is most affected is hidden in a region of high uncertainty and incompleteness. An example of this is seen in the CMD of the Carina dwarf spheroidal, where the RGB reveals nothing of the complex star formation history clearly seen in other regions of the CMD (Smecker-Hane et al. 1994). Beyond an age of 3 Gyr, large numbers of stars could be added with very little impact on the observed CMD.

Figure 19 shows the resulting star formation history for RGB stars in the WF2 field. Instead of giving error bars, which are very difficult to quantify in the absence of a clearly unique solution, we show several possible solutions. The number of stars at the tip of the RGB constrains the younger age limits and rates (600–800 Myr), and the number of stars at the base of the observed CMD constrains the total number of stars formed beyond 800 Myr. In order to match the observed numbers, our model requires a large fraction of stars to have been formed 600–800 Myr ago; this is the large spike in Figure 19. The reasons for this constraint can be clearly seen in Figure 18. The tip of the RGB as observed does not allow large numbers of stars younger than 600 ± 50 Myr, because this would put too many stars in the tip of the RGB and would also require more blue stars than are seen in the observed CMD. This can be seen in the 400–550 Myr models. The demarcation at 800 Myr between the epoch of intense star formation and lower rates at earlier times is not well constrained. Furthermore, the spike of star formation could have begun as early as 1.2 Gyr; the broader the starburst, the lower the amplitude that is needed. The large number of AGB stars, whose ages would be expected to be in the range 1–5 Gyr (see Fig. 15), may argue for the longer episode of star formation. Beyond 1 Gyr the uncertainties in matching the CMD become large because the stars formed at these ages all lie at the same positions on the CMD, and any combination of star formation rates and times can be accommodated provided that the end result does not create too many stars. That is, the formation rate of stars older than 800 Myr needs to remain relatively low but is not otherwise well constrained.

7.3. *Final Model*

The final composite star formation history for all four WFPC2 fields is shown in Figure 20, and the best model CMD is shown in Figure 21, together with the corresponding observations. In summary, we find that there was a very intense star formation episode that ended about 600 Myr ago and began at least 800 Myr ago—and possibly as early as 1.2 Gyr ago. The exact amplitude of the starburst depends on how long the episode lasted; what is shown in Figure 20 is the short-duration, high-amplitude version. Star formation 1–2 Gyr ago was lower than this, but the exact nature of the star formation history for this period is undetermined. Older than 3 Gyr, the star formation history is completely unconstrained. In addition, the star formation rate between 50 and 600 Myr must have been relatively low. (The dip in the star formation rate near zero age shown in Figure 20 is without meaning; our modeling does not deal well with young, massive stars.) The amplitude of the star formation activity 600–800 Myr ago was ~ 30 times higher than it was at other ages for the model shown in Figure 20. If the galaxy is actually farther away by 0.5 mag, a possibility that was considered in § 7.1, the starburst also becomes less intense and is spread out over an even longer interval of time.

8. DISCUSSION

For a distance of 4.5 Mpc and an $E(B-V)$ of 0.04, the galaxy-wide luminosity in Hα in UGC 6456 is 1.8×10^{39} ergs s^{-1}. The current (<10 Myr) star formation rate deduced from this is 0.013 $M_\odot$ yr^{-1}, assuming a Salpeter stellar IMF from 0.1 to 100 $M_\odot$ (Hunter & Gallagher 1986). The star formation rate is 0.0037 $M_\odot$ yr^{-1} kpc^{-2} over an area within $D_{25} = 1.9$ kpc (de Vaucouleurs et al. 1991, hereafter RC3). This star formation rate is only modestly higher

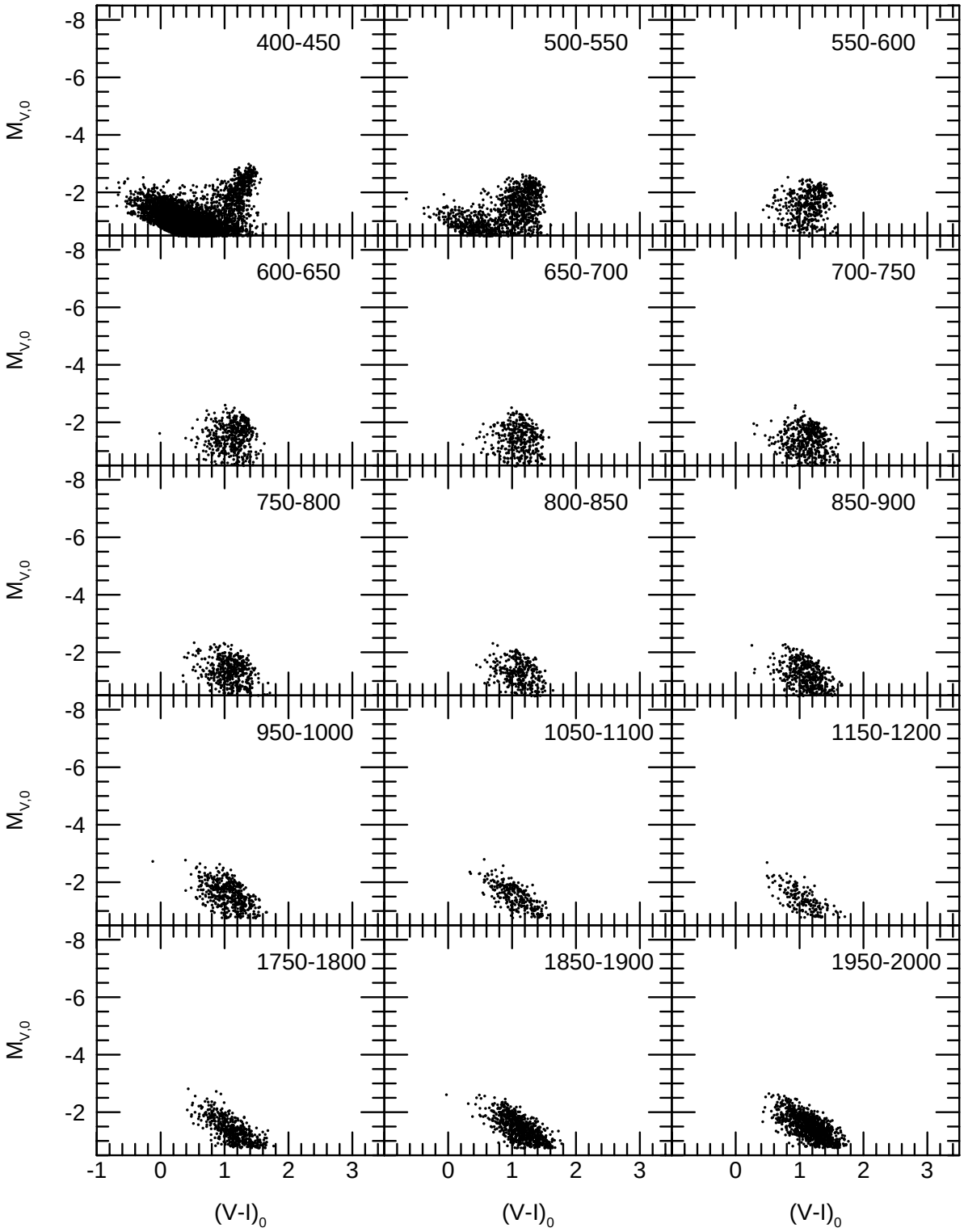

FIG. 18.—Star formation models for 400–2000 Myr in steps of 50 Myr. Each model represents 50 Myr of star formation in the epoch given at the top right of each plot. The model is corrected for incompleteness and convolved with the photometric uncertainties determined from the data.

than the median for a typical, noninteracting Im galaxy, but not at all unusual among a sample of 51 irregulars (Hunter 1998). With an H I gas content of $7.5 \times 10^7\ M_\odot$ (Thuan & Martin 1981, corrected to a distance of 4.5 Mpc), the timescale to exhaust the neutral gas (H plus He) at the present formation rate is 8 Gyr. The total blue luminosity of the galaxy is $M_B = -14.3$ (RC3), and from our *HST* images we find that $(U-V)_0 = 0.16$ and $(V-I)_0 = 0.63$.

We find that what is especially interesting about UGC 6456 is a former starburst that occurred over 600 Myr ago, rather than its current activity. X-ray emission associated with UGC 6456 has been detected by Papaderos et al. (1994). They find a core centered on the galaxy and three elongated structures, which they interpret as hot gas flowing out from the center of the galaxy caused by the present star formation activity. However, we have found

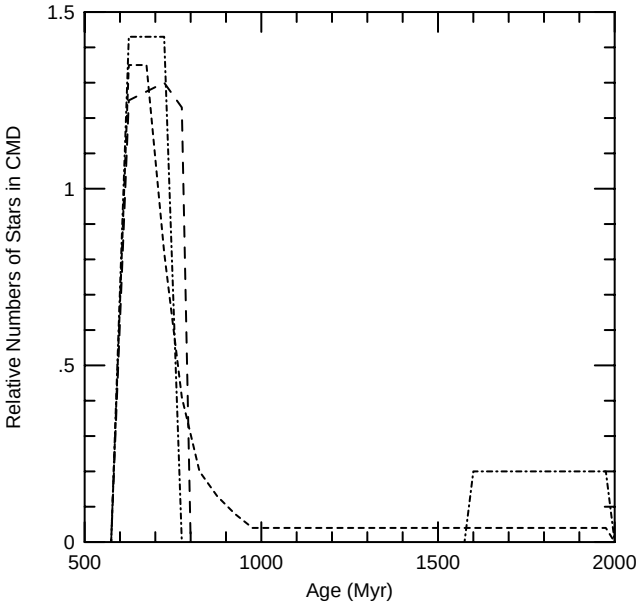

FIG. 19.—Rough star formation epochs determined from the RGB and main sequence of WF2. The vertical axis is number of stars formed in each 50 Myr time bin. A Salpeter initial mass function from 0.1 to 100 $M_\odot$ is assumed. Because the different CCDs have similar RGBs, this star formation history will scale for the other CCDs. The normalization here is roughly that of the entire WFPC2 field of view.

that the current star formation activity is, in fact, fairly modest, and a more likely scenario would be that the X-ray emission is associated with the star forming event that occurred 600 Myr ago. Is the timescale for that starburst consistent with that for the production of the hot X-ray gas? The minimum timescale for the formation of the X-ray lobes is several Myr, according to Papaderos et al., while the cooling time is greater than 100 Myr. Potentially hot gas that was produced by supernovae in the 10–20 Myr after the burst 600 Myr ago would not yet have cooled.

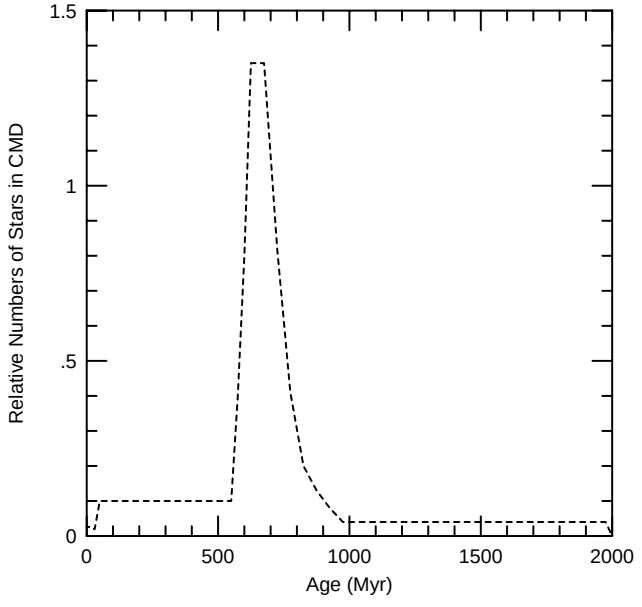

FIG. 20.—Final best star formation history for all four CCDs

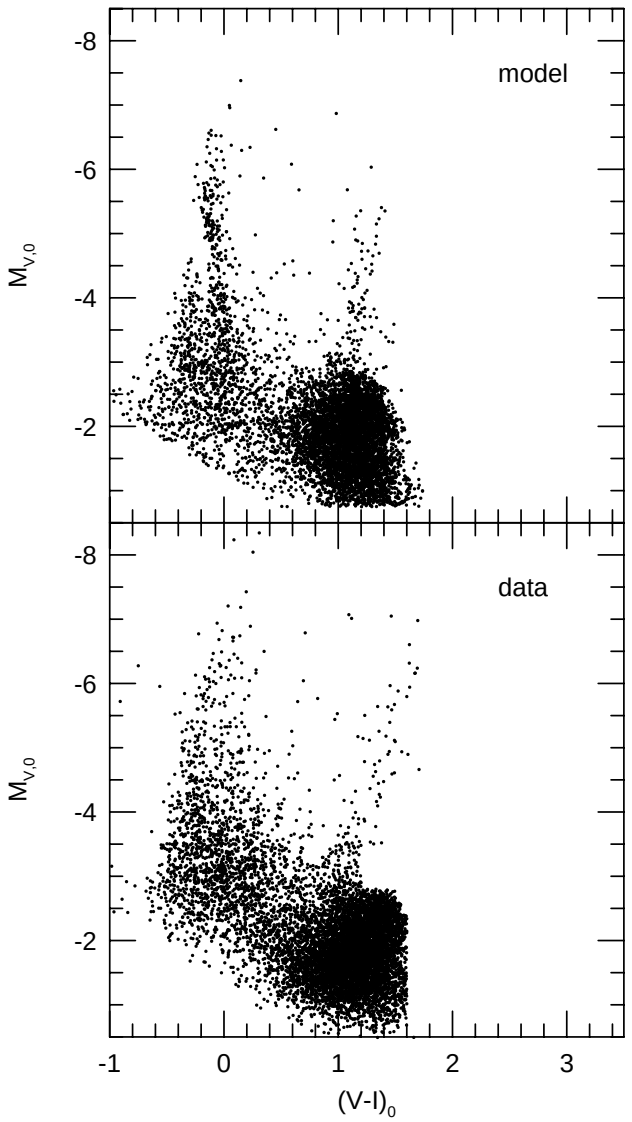

FIG. 21.—Best model CMD. The observed CMD is also shown to aid in comparison.

However, the X-ray lobes would have to be older than the several Myr deduced from simple kinematic arguments.

UGC 6456 must have looked very different in the past compared with what we see today. If that starburst lasted 200 Myr, we find a star formation rate about 30 times greater than the current rate. Babul & Ferguson (1996) have constructed starburst models of dwarf galaxies, and their Figure 6 shows that a 10^9 $M_\odot$ galaxy with a star formation rate of 3 $M_\odot$ yr^{-1} would fade by about 2 mag after 600 Myr. For UGC 6456, we have a factor of 10 smaller total mass as well as a factor of 10 smaller star formation rate. If the models scale simply by these two factors, we would expect UGC 6456 to have also been something like 2 mag brighter during its starburst. Thus, the galaxy would have been roughly -16 in M_B.

There has been some speculation that the excess in faint blue galaxies found in deep imaging could be dwarf irregular or dwarf elliptical galaxies undergoing starbursts (e.g., Babul & Ferguson 1996; Babul & Rees 1992). These galaxies are found at about $B \geq 24$ and redshifts of 0.5 to 1.

For a Hubble constant of 75 km s^{-1} Mpc^{-1}, a galaxy at a redshift $Z = 0.5$ having an apparent B magnitude of 25 would have an absolute B magnitude of -16, comparable to that of UGC 6456. Perhaps these distant, faint blue galaxies were going through a starburst phase similar to that which occurred in UGC 6456 more recently.

This research was supported in part by NASA grant NAS 5-25421 to the WFPC Investigation Definition Team. We thank P. Massey for obtaining the spectra for us. We would also like to thank K. Mighell, T. Armandroff, and A. Saha for a number of very helpful conversations.

REFERENCES

Babul, A., & Ferguson, H. C. 1996, ApJ, 458, 100
Babul, A., & Rees, M. J. 1992, MNRAS, 255, 346
Bertelli, G., Bressan, A., Chiosi, C., Fagotto, F., & Nasi, E. 1994, A&AS, 106, 275
Burstein, D., & Heiles, C. 1984, ApJS, 54, 33
Carozzi, N., Chamaraux, P., & Duflot-Augarde, R. 1974, A&A, 30, 21
Charbonnel, C., Meynet, G., Maeder, A., Schaller, G., & Schaerer, D. 1993, A&AS, 101, 415
Da Costa, G. S., & Armandroff, T. E. 1990, AJ, 100, 162
de Vaucouleurs, G., de Vaucouleurs, A., Corwin, H. G., Jr., Buta, R. J., Paturel, G., & Fouqué, P. 1991, Third Reference Catalogue of Bright Galaxies (New York: Springer) (RC3)
Fanelli, M. N., O'Connell, R. W., & Thuan, T. X. 1988, ApJ, 334, 665
Freedman, W. L. 1988, AJ, 96, 1248
French, H. B. 1980, ApJ, 240, 41
Gallart, C., Aparicio, A., Chiosi, C., Bertelli, G., & Vílchez, J. M. 1994, ApJ, 425, L9
Gordon, D., & Gottesman, S. T. 1981, AJ, 86, 161
Holtzman, J. 1990, PASP, 102, 806
Holtzman, J. A., et al. 1995, PASP, 107, 156
Hunter, D. A. 1995, in The Fifth Mexico-Texas Conference on Astrophysics, ed. M. Peña & S. Kurtz (Rev. Mexicana Astron. Astrofis. Ser. Conf., 3) (México, D.F.: Inst. Astron., Univ. Nac. Autónoma México), 1
———. 1998, in preparation
Hunter, D. A., Baum, W. A., O'Neil, E. J., Jr., & Lynds, R. 1996, ApJ, 456, 174
Hunter, D. A., & Gallagher, J. S. 1986, PASP, 98, 5
Hunter, D. A., Shaya, E. J., Holtzman, J. A., Light, R. M., O'Neil, E. J., Jr., & Lynds, R. 1995, ApJ, 448, 179
Izotov, Yu. I., Thuan, T. X., & Lipovetsky, V. A. 1997, ApJS, 108, 1
Kunth, D. 1987, Sci. Rep. Tôhoku Univ., 7, 353
Kurucz, R. L. 1991, in Stellar Atmospheres, ed. L. Crivellari, I. Hubeny, & D. G. Hummer (NATO ASI Ser. C, 341) (Dordrecht: Kluwer), 441
Lee, M. G. 1995, AJ, 110, 1129
Lee, M. G., Freedman, W. L., & Madore, B. F. 1993, ApJ, 417, 553
Loose, H.-H., & Thuan, T. X. 1985, in Star-forming Dwarf Galaxies and Related Objects, ed. D. Kunth, T. X. Thuan, & J. Trân Thanh Vân (Gif-sur-Yvette: Ed. Frontières), 73
Massey, P., Lang, C. C., Degioia-Eastwood, K., & Garmany, C. D. 1995, ApJ, 438, 188
McCray, R., & Kafatos, M. 1987, ApJ, 317, 190
Papaderos, P., Fricke, K. J., Thuan, T. X., & Loose, H.-H. 1994, A&A, 291, L13
Papaderos, P., Loose, H.-H., Thuan, T. X., & Fricke, K. J. 1996, A&AS, 120, 207
Saha, A., Sandage, A., Labhardt, L., Schwengeler, H., Tammann, G. A., Panagia, N., & Macchetto, F. D. 1995, ApJ, 438, 8
Sakai, S., Madore, B. F., & Freedman, W. L. 1996, ApJ, 461, 713
Salpeter, E. E. 1955, ApJ, 121, 161
Schaller, G., Schaerer, D., Meynet, G., & Maeder, A. 1992, A&AS, 96, 269
Schild, R. 1977, AJ, 82, 337
Schulte-Ladbeck, R. E., Crone, M. M., & Hopp, U. 1998, ApJ, 493, L23
Seaton, M. J. 1975, MNRAS, 170, 475
Shull, J. M., & Saken, J. M. 1995, ApJ, 444, 663
Smecker-Hane, T. A., Stetson, P. B., Hesser, J. E., & Lehnert, M. D. 1994, AJ, 108, 507
Stetson, P. B. 1987, PASP, 99, 191
Thuan, T. X., & Martin, G. E. 1981, ApJ, 247, 823
Thuan, T. X., Williams, T. B., & Malumuth, E. 1987, in Starbursts and Galaxy Evolution, eds. T. X. Thuan, T. Montmerle, & J. Trân Thanh Vân (Gif-sur-Yvette: Ed. Frontières), 151
Tolstoy, E., & Saha, A. 1996, ApJ, 462, 672
Tosi, M., Greggio, L., & Focardi, P. 1991, AJ, 102, 951
Tully, R. B., Boesgaard, A. M., Dyck, H. M., & Schempp, W. V. 1981, ApJ, 246, 38
Vanzi, L., Rieke, G. H., Martin, C. L., & Shields, J. C. 1996, ApJ, 466, 150
Weaver, R., McCray, R., Castor, J., Shapiro, P., & Moore, R. 1977, ApJ, 218, 377